

Lethal Giant Disc is a target of Cdk1 and regulates ESCRT-III localization during germline stem cell abscission

Catherine Hermant, Neuza Reis Matias, Pascale Michel-Hissier, Jean-René Huynh* and Juliette Mathieu*

ABSTRACT

Abscission is the final step of cytokinesis that allows the physical separation of sister cells through the scission of the cellular membrane. This deformation is driven by ESCRT-III proteins, which can bind membranes and form dynamic helices. A crucial step in abscission is the recruitment of ESCRT-III proteins at the right time and place. Alix is one of the best characterized proteins that recruits ESCRT-III proteins from yeast to mammals. However, recent studies *in vivo* have revealed that pathways acting independently or redundantly with Alix are also required at abscission sites in different cellular contexts. Here, we show that Lgd acts redundantly with Alix to properly localize ESCRT-III to the abscission site in germline stem cells (GSCs) during *Drosophila* oogenesis. We further demonstrate that Lgd is phosphorylated at multiple sites by the CycB/Cdk1 kinase. We found that these phosphorylation events potentiate the activity of Shrub, a *Drosophila* ESCRT-III, during abscission of GSCs. Our study reveals that redundancy between Lgd and Alix, and coordination with the cell cycle kinase Cdk1, confers robust and timely abscission of *Drosophila* germline stem cells.

KEY WORDS: ESCRT-III, Shrub, CHMP4, ALIX, Lgd, Germline stem cell, CC2D1

INTRODUCTION

ESCRT-III (Endosomal Sorting Complex Required for Transport) are small proteins that are able to both polymerize into helices and drive membrane deformation for many cellular events, such as endosome maturation, retroviral budding, nuclear envelope sealing or cytokinetic abscission (Andrade and Echard, 2022; Pfitzner et al., 2021; Stoten and Carlton, 2018; Vietri et al., 2019). A key question is understanding how ESCRT-III proteins are targeted to the right place at the right time within the same cell for each event. Several targeting factors have been identified for different cellular processes. In the case of cytokinetic abscission, ALiX (ALG-2 interacting protein X) was shown to play a major role in binding and recruiting ESCRT-III proteins at the intercellular bridge that links the two daughter cells at the end of cytokinesis (Addi et al., 2020; Carlton and Martin-Serrano, 2007; Elia et al., 2011; Guizetti et al., 2011; Morita et al., 2007). However, ALiX mutant flies and Alix (*Pdcd6ip*; ALG-2 interacting protein) mutant mice are viable (Eikenes et al., 2015; Laporte et al., 2017), and additional pathways


were recently uncovered to act redundantly or independently of ALiX for the recruitment of ESCRT-III at the abscission site. In HeLa cells, it has been shown that CHMP4B (charged multivesicular body protein 4B), a mammalian ESCRT-III, is also recruited via an ESCRT-I-ESCRT-II-CHMP6 pathway, in parallel to ALiX (ALG-2-interacting protein X) (Christ et al., 2016; Goliand et al., 2014). Furthermore, in the eye lens of fish, mouse and human, the lipid kinase PI3K-C2 α has been shown to be required together with ESCRT-II to recruit ESCRT-III to the midbody for the timely abscission of HeLa cells. Interestingly, this recruitment pathway is non-redundant, as ALiX is poorly expressed in these cells (Gulluni et al., 2021). Therefore, in addition to having different targeting factors of ESCRT-III for different membrane-deformation events within the same cell, different recruitment mechanisms exist for the same fission event, such as abscission, in different cell types.

Drosophila germline stem cells (GSCs) are a powerful tool for studying abscission in an intact organ. Indeed, *Drosophila* genetic tools can be used at the single stem cell level to study the function of any gene throughout the GSC cell cycle. Furthermore, GSC abscission can be easily visualized with a germline-specific organelle called the fusome, which is made of ER-derived vesicles (Mathieu and Huynh, 2017). In wild-type conditions, GSCs are linked to a single daughter cell called a cystoblast (CB) by a linear fusome. The fusome becomes severed at the end of an unusually long abscission, happening at the G2 phase of the next GSC cell cycle (de Cuevas and Spradling, 1998; Mathieu and Huynh, 2017; Matias et al., 2015; Villa-Fombuena et al., 2021) (Fig. 1A,B, Fig. S1A). In mutant conditions when GSC abscission is delayed, the next round of mitosis occurs while GSC/CB pairs are still linked by intercellular bridges, giving rise to four interconnected cells (stem-cyst), which leads ultimately to the formation of egg chambers made from 32 cells instead of 16 (Mathieu et al., 2013) (Fig. S1B). The formation of stem-cysts can easily be visualized by the formation of branched fusomes, and 32-cell egg chambers are also a simple read-out of abscission delays in GSCs. Such phenotypes demonstrate that genes such as ALiX, *shrub* (a *Drosophila* ESCRT-III, the single CHMP4 protein family homolog), *Cyclin B* or *lethal giant discs* (*lgd*) are required for GSC abscission (Eikenes et al., 2015; Mathieu et al., 2013; Matias et al., 2015). However, how these different genes and pathways cooperate to regulate GSC abscission remains unclear.

Lethal (2) Giant Disc (Lgd) is the single *Drosophila* homologue of mammalian CC2D1A and CC2D1B, and binds directly to ESCRT-III proteins Shrub/CHMP4 (Baeumers et al., 2022; McMillan et al., 2017; Troost et al., 2012). On the one hand, structural studies suggested that Lgd inhibits ESCRT-III polymerization by sequestering Shrub/CHMP4 in the cytoplasm (McMillan et al., 2017). In agreement, in mammalian cells lacking CC2D1B, CHMP4B is recruited precociously at the reforming nuclear envelope (Ventimiglia et al., 2018). On the other hand, genetic studies have found a positive role for Lgd in abscission and endosome maturation *in vivo* (Baeumers et al., 2022; Clarke et al., 2022; Matias et al., 2015; Troost et al., 2012). For

Collège de France, PSL Research University, CNRS Biologie, INSERM, Center for Interdisciplinary Research in Biology, Paris 75005, France.

*Authors for correspondence (jean-rene.huynh@college-de-france.fr; juliette.mathieu@college-de-france.fr)

 C.H., 0000-0002-3906-2546; J.-R.H., 0000-0002-4078-399X; J.M., 0000-0002-7152-4245

Handling Editor: Swathi Arur

Received 29 August 2023; Accepted 14 March 2024

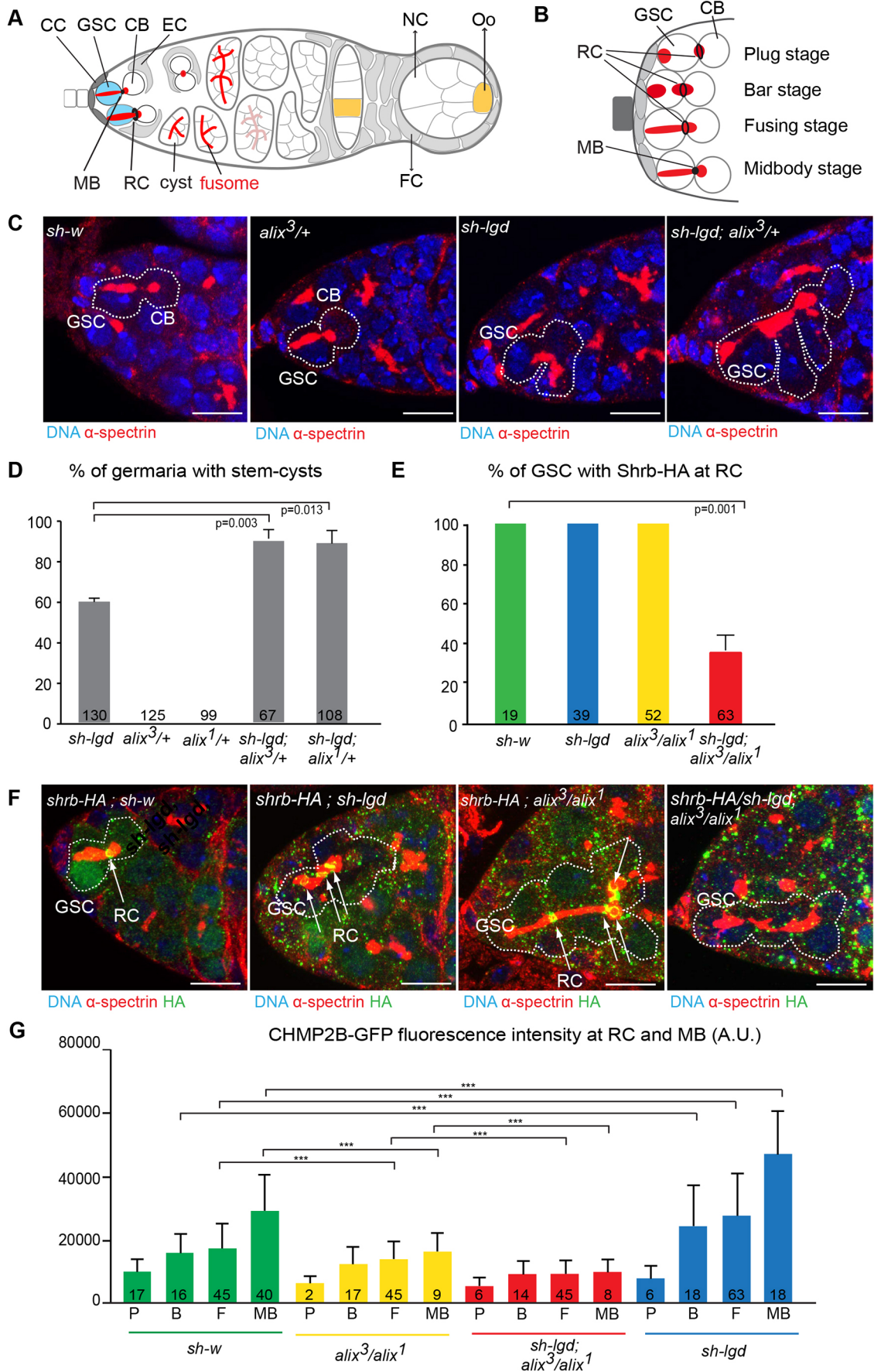


Fig. 1. See next page for legend.

Fig. 1. Lgd and Alix act redundantly to localize ESCRT-III at the ring canal. (A) Schematic of a germarium. At the anterior tip, the germline stem cells (GSCs, blue) divide asymmetrically to produce a GSC and a cystoblast (CB). Each CB goes through four rounds of synchronous and incomplete divisions to form a cyst of 16 interconnected cells: 15 nurse cells (NCs) and one oocyte (Oo, yellow). Somatic caps cells (CCs) maintain GSC stemness, while escort cells (ECs) promote CB differentiation. The germline cyst is encapsulated by somatic follicular cells (FCs) and buds out of the germarium. The fusome (red) is a germline-specific organelle present in the GSCs, CBs and the cysts. GSCs and CBs remain connected by a ring canal (RC) until completion of abscission, when the midbody (MB, black) forms a bulge on the fusome between the GSC and the CB. Anterior is on the left; posterior is on the right. (B) Schematic of the GSC stages analyzed in this study. The GSCs (on the left) and their daughter CBs (on the right) are linked by RCs at the plug stage then at bar and fusing stages, and finally by a midbody (MB) at the midbody stage. (C) Confocal images of germaria from females immunostained for α -spectrin (red). Genotypes are indicated. *sh-w* stands for sh-RNA directed against the white gene (unrelated to abscission) and is the control genotype. Dashed lines surround GSC/CB pairs or stem cysts. The anterior-most GSC is indicated. Scale bars: 10 μ m. (D) The fraction of germaria exhibiting at least one stem-cyst (*y*-axis). Genotypes are on the *x*-axis. Numbers of germaria analyzed are indicated. Data are mean \pm s.e.m. of three experiments. *P* values are derived from unpaired *t*-tests. (E) Fraction of GSCs exhibiting a stem-cyst or a GSC/CB pair, the RCs of which are stained for Shrub-HA. The numbers of GSCs analyzed are indicated. Data are mean \pm s.e.m. of three experiments. Numbers of GSCs analyzed are indicated. The *P* value is derived from unpaired *t*-tests. Genotypes are on the *x*-axis. *sh-w* stands for sh-RNA directed against the white gene (unrelated to abscission), and is the control genotype. (F) Confocal images of germaria obtained from females expressing *shrub-HA* under the control of *nos-GAL4* in combination with *sh-w* (sh-RNA directed against the white gene as a control), *sh-lgd* and/or *alix3/alix1* immunostained for α -spectrin (red) and HA (shrub-HA, green). Dashed lines surround GSC/CB or stem-cysts. Anterior GSCs are indicated. Arrows indicate the RCs stained for Shrub-HA. Scale bars: 10 μ m. (G) Fluorescence intensity (arbitrary unit, A.U.) of CHMP2B-GFP at the RC of a GSC [at stages plug (P), bar (B) and fusing (F)] or at the midbody (MB) of GSCs in control (*sh-w*, for short-hairpin against white gene, green), *alix³/alix¹* (yellow), *alix³/alix¹+sh-lgd* (red) or *sh-lgd* (blue) ovaries. Numbers of GSCs analyzed are indicated. ****P*<0.0001 (Wilcoxon-Mann-Whitney test).

example, in worms, Lgd is required for the stable recruitment and/or polymerization of ESCRT-III subunits during endosome maturation (Clarke et al., 2022). Here, we have addressed the function of Lgd during abscission of the GSCs. We demonstrate that Lgd acts redundantly with ALiX to localize Shrub and CHMP2B at the intercellular bridge. We also find that Lgd is phosphorylated by Cdk1 on conserved residues, and show that these phosphorylation events potentiate Lgd activity on Shrub.

RESULTS

ALiX and Lgd cooperate to localize ESCRT-III at GSCs abscission site

We and others showed that GSCs homozygous mutant for a strong allele of *lgd* (*lgd^{d7}*) induced the formation of egg chambers with 32 cells (Matias et al., 2015; Morawa et al., 2015). We further showed that *lgd* mutation induced a strong delay in GSC abscission and the formation of stem-cysts in 70% of cases. Here, we have expressed (specifically in GSCs) a short-hairpin (sh) RNA targeting *lgd* (*sh-lgd*), and found that it also led to the formation of stem-cysts in 60% of germaria (Fig. 1C,D), confirming the efficiency and specificity of the *sh-lgd* line. We then analyzed the localization of Shrub in *sh-lgd* GSCs and found that in 100% (*n*=39) of cases, Shrub was still localized to the GSC ring canals (RCs), regardless of whether or not stem-cysts were formed (Fig. 1E,F, Fig. S1D,E). This result indicates that factors other than Lgd recruit Shrub at GSC abscission site.

ALiX mutant flies have previously been shown to form stem-cysts, and ALiX was proposed to recruit Shrub during GSC abscission (Eikenes et al., 2015). We thus examined Shrub localization in *alix¹/alix³* GSCs, and surprisingly found that Shrub was present in 100% (*n*=52) of cases, indicating again that additional factors helped to recruit Shrub at abscission sites (Fig. 1E,F, Fig. S1D,E). We then depleted both *alix* and *lgd* in dividing GSCs and observed that Shrub was not detected in 70% (*n*=63) of cases (Fig. 1E,F, Fig. S1D,E). This result indicated that Lgd and ALiX act redundantly to localize Shrub at the abscission site. In addition, we found that removing a single copy of *alix* (with two different alleles, *alix¹* and *alix³*) in a *sh-lgd* background was sufficient to significantly increase the number of stem-cysts from 60% to 80% in germaria (Fig. 1D). In contrast, removing one copy of *alix* in a wild-type background had no effect on its own (Fig. 1D). These results demonstrated that Lgd and ALiX act redundantly for Shrub localization and cooperate for the completion of GSC abscission in *Drosophila*.

Shrub-HA immunodetected in ovaries is overexpressed from a transgene under the control of the *nos-GAL4* driver. Therefore Shrub-HA levels are not a quantifiable readout of ESCRT-III levels at the intercellular bridge. Instead, we used a GFP-tagged version of CHMP2B (another *Drosophila* ESCRT-III) expressed under the control of its endogenous promoter and quantified the fluorescence intensity at the ring canal at different stages of GSCs abscission. We used the shape of the fusome (plug, bar, fusing and midbody, Fig. 1B) to stage the advancing steps of GSC cytokinetic abscission (Ables and Drummond-Barbosa, 2013). We observed a gradual increase of CHMP2B fluorescent signal at the ring canal of control GSCs (Fig. 1G). In *alix¹/alix³* transheterozygous flies, CHMP2B levels were significantly decreased in late stages of abscission compared with the *sh-w* control (Fig. 1G). We found an even stronger decrease of CHMP2B signal when both ALiX and Lgd were knocked down (Fig. 1G). This result confirmed the redundant role of Lgd and ALiX for the recruitment of ESCRT-III proteins during GSCs abscission. Unexpectedly, we observed that CHMP2B levels were increased in *sh-lgd* single depletion compared with *sh-w* control (Fig. 1G). This result indicated that Lgd negatively regulates CHMP2B levels during abscission, as proposed during nuclear envelope repair in mammalian cells (Ventimiglia et al., 2018). *lgd* thus appears to have opposite functions on ESCRT-III localization in single depletion versus co-depletion with ALiX. We therefore asked whether these two functions could be mediated by different pools of Lgd proteins.

Lgd is phosphorylated by Cdk1

Members of the conserved Lgd/CC2D1 protein family contain four repeats of a DM14 (*Drosophila Melanogaster* 14) domain, followed by a lipid interacting C2 domain and many putative sites of post-translational modifications (Fig. 2A,B). The third DM14 domain binds Shrub on its homo-polymerization surface (McMillan et al., 2017). We identified 14 putative Cdk1 consensus sites (S/Tp-P) in the *Drosophila* Lgd sequence. Thirteen sites were located between two DM14 domains, and one site was in the C2 domain (Fig. 2B, blue arrowheads). Importantly, the positions of these sites are highly conserved in the two mammalian homologs CC2D1A and CC2D1B, suggesting functional significance (Fig. 2B, black arrowheads) and we note that one of these sites in CC2D1A (also known as Aki1) had previously been shown to be phosphorylated by Cdk1 in mammalian cell culture (Nakamura et al., 2010). To test whether these sites were phosphorylated *in vivo*, we immunoprecipitated a GFP-tagged Lgd protein expressed in *Drosophila* embryos, and sequenced it by mass spectrometry (Fig. 2A, construct 2). Five sites were phosphorylated at positions S225, T239, T242, S254 and S474 (Fig. 2B; Fig. S2, green

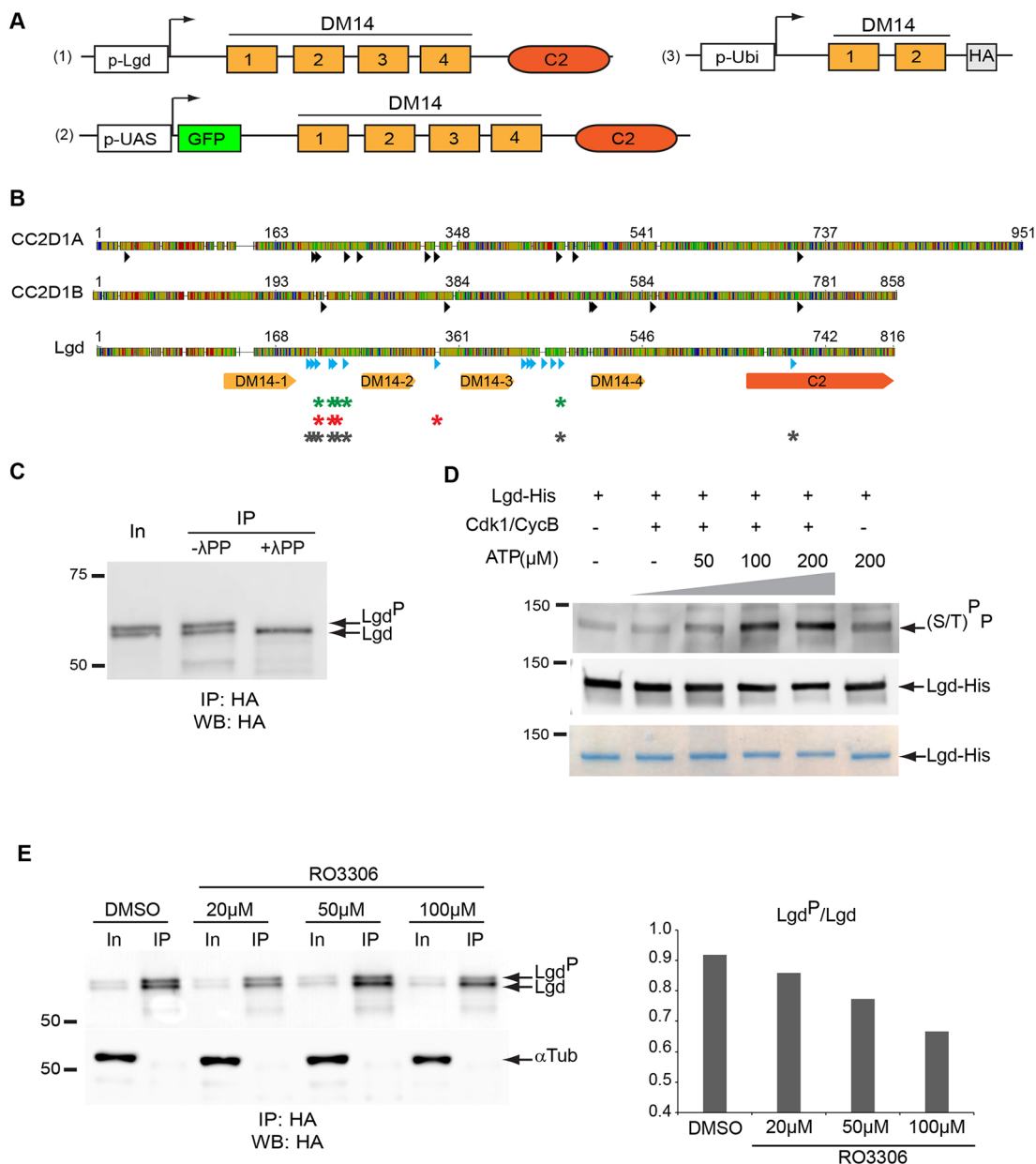


Fig. 2. Lgd is phosphorylated *in vivo* and *in vitro* by Cdk1. (A) (1) Schematic of *Drosophila melanogaster* Lgd endogenous locus showing the promoter (p-Lgd), four DM14 domains (light orange) and one C2 domain (dark orange). (2) Schematic of the GFP-tagged Lgd construct expressed in fly embryos for biochemistry experiments. Expression was driven by a Gal4 inducible UAS promoter (p-UAS) and GFP was fused at the N-terminal part. (3) Schematic of the HA-tagged mini-Lgd construct expressed in *Drosophila* S2 cells for biochemistry experiments. The N-terminal part of Lgd cDNA, encompassing DM14 domains 1 and 2, was fused to HA and expressed under the control of the ubiquitin promoter (p-Ubi). This shorter form of Lgd (but not the full length) allowed the visualization of two distinct bands upon gel separation (see C and E). (B) Alignment of the protein sequences of human CC2D1A and CC2D1B, and the unique *Drosophila melanogaster* homolog Lgd. The black and blue arrowheads indicate Cdk1 consensus sites of phosphorylation (S/T*P). Fourteen putative sites for Cdk1 phosphorylation are found in the *Drosophila* sequence at positions S217, T222, S225, T239, T242, S254, T347, T436, S442, S445, T457, T465, S474 and T712. Green asterisks at positions S225, T239, T242, S254 and S474 correspond to the five phosphorylation events detected in embryos expressing GFP-Lgd. Red asterisks at positions S225, T239, T242 and T347 correspond to four phosphorylation events detected on purified Lgd protein treated by Cdk1/CycB and ATP in the kinase assay (see D). Grey asterisks at positions S217, T222, S225, T239, T242, S254, S474 and S712 correspond to the eight phosphorylation events detected on GFP-Lgd purified from *nos-GAL4*, *UAS-GFP-Lgd-WT* ovaries. (C) Immunoblot of input (In) or immunoprecipitated (IP) mini-Lgd-HA protein from S2 cells transfected with mini-Lgd-HA expression vector. IP eluates were treated (+λPP) or not (-λPP) with λ phosphatase. Membranes were blotted with anti-HA antibody. This immunoblot is representative of four experiments. (D) Immunoblots and Coomassie Blue staining of purified Lgd-His protein submitted to a Cdk1/CycB kinase assay with increasing ATP concentrations. Membranes were blotted with MPM2, which recognized (S/T)^P-P, the phosphorylated form of Cdk1 consensus site, and with anti-His antibody. This immunoblot is representative of three experiments. A sample of Lgd-His treated with Cdk1/CycB plus 200 μM ATP (similar to 5th lane) was used for mass spectrometry. The identified phosphorylated sites are indicated by red asterisks in B. The control for this mass spectrometry experiment corresponded to a sample treated with ATP only (similar to 6th lane). (E) Left: immunoblots of input (In) or immunoprecipitated (IP) mini-Lgd-HA protein from S2 cells transfected with mini-Lgd-HA expression vector and treated or not with the Cdk1 inhibitor RO3306. Membranes were blotted with anti-HA (top) and anti-α-Tubulin (bottom) antibodies. This immunoblot is representative of four experiments. Right: ratios of Lgd^P band intensity/Lgd band intensities at increasing RO3306 concentrations. DMSO alone served as control.

Table 1. Peptides identified on LgdGFP from embryos

| Peptide sequence | Mascot score | Q value | Binomial peptide score | Best site probability | PSM modification position in protein | Mascot score control |
|---|--------------|---------|------------------------|---|---|----------------------|
| K. SINVDIPPEVSVKPIGGQAPPVPAEESPAP STPASPPVPSR. A | 21 | 0 | 281 | S36(P):99.97 | 1×Phospho [S225(100)] | - |
| R. AAPDPPTGTPVEPTTSVAPTSPPNPLVTQMR. S | 20 | 0.00017 | 177 | T10 (P): 99.94; S22(P): 97.82; M31(Ox): 100 | 2×Phospho [T242(99.9); S254(97.8)] | - |
| R. AAPDPPTGTPVEPTTSVAPTSPPNPLVTQMR. S | 20 | 0.00017 | 138 | T7 (P): 48.63; T10(P): 48.63; M31(Ox): 100 | 1×Phospho [T239] <50 1×Phospho [T242] <50 | - |
| R. KAPSPKPKKE LTR. T | 25 | 0.00427 | 105 | S4(P): 100 | 1×Phospho [S474(100)] | - |

Lgd is phosphorylated *in vivo*. Mass spectrometry was performed on embryos expressing pUAS-GFP-Lgd-WT and pUAS-GFP (control) under the control of nos-GAL4. Samples were processed for immunoprecipitation and then treated with trypsin. A list of peptides detected and their phosphorylation is indicated, with their Mascot score, Q-value, binomial peptide score, best site probability, PSM modification position in protein and Mascot score for the control provided by the Proteome Discoverer 2.1 program. Analysis detected phosphorylation modifications at positions S225, T239, T242, S254 and S474 (green stars in Fig. 2B).

stars; Table 1), four of which were clustered between the DM14-1 and DM14-2 domains. These five sites were also detected as phosphorylated in germline cell extracts expressing GFP-Lgd (Fig. 2B, Fig. S2).

To confirm Lgd phosphorylation *in vivo*, we expressed an N-terminal form of Lgd containing these four clustered sites tagged with HA in *Drosophila* S2 cells (also known as mini-Lgd, Fig. 2A, construct 3). After immunoprecipitation, mini-Lgd was treated with λ -phosphatase. Two bands were detected by immunoblot in the control lanes (Fig. 2C). The higher molecular weight band was sensitive to λ -phosphatase as it disappeared after treatment (Fig. 2C). This result indicated that mini-Lgd was present in both phosphorylated (upper band) and non-phosphorylated (lower band) forms in *Drosophila* cells.

To test whether Cdk1 could phosphorylate these sites *in vivo*, we first tested the ability of recombinant Cdk1/CycB to directly phosphorylate purified Lgd protein *in vitro*. His-tagged full-length Lgd protein was produced in insect cells, and incubated with Cdk1/CycB at increasing ATP concentrations. Reactions were then analyzed by immunoblot using an anti S/Tp-P antibody to reveal phosphorylated Lgd. We observed a gradual increase in the amount of phosphorylated Lgd, which followed the gradual increase of ATP concentrations (Fig. 2D). To confirm that Cdk1 had indeed phosphorylated full-length His-Lgd at these putative sites, we sequenced the product of the kinase assay by mass spectrometry. In the *in vitro* assay, we found four phosphorylated sites, S225, T239,

T242 and T347, three of which corresponded to sites identified *in vivo* (Fig. 2B, red stars; Fig. S2 and Table 2).

Finally, we treated S2 cells with a Cdk1 inhibitor (RO3306) and assessed the amount of phosphorylated HA-mini-Lgd by immunoblot (Fig. 2E). We observed that the fraction of phosphorylated versus non-phosphorylated Lgd decreased as the amount of Cdk1 inhibitor increased (Fig. 2E). This result indicated that Lgd phosphorylation depended on Cdk1 activity *in vivo*. Altogether, these experiments demonstrate that Lgd is phosphorylated by Cdk1 *in vivo*, and suggest that different pools of phosphorylated and unphosphorylated Lgd could co-exist in GSCs.

Phosphorylation-dependent localization of Lgd during GSC abscission

Next, to address whether different pools of Lgd were present in GSCs, we tagged wild-type, phosphomimetic and non-phosphorylatable variants of Lgd with GFP, and analyzed their localization. We generated transgenic flies expressing full-length Lgd under the control of its endogenous regulatory regions (419 bp in 5' as a promoter -p*lgd*- and 416 bp in the 3'UTR). All transgenes were inserted at the same genomic locus. In Lgd14A, all putative phosphorylation sites of Cdk1 were mutated into alanine to preclude any phosphorylation by Cdk1. In Lgd5A, only the five sites identified by mass spectrometry in embryo and ovarian extracts were mutated into alanine; and in Lgd5E, these same sites were replaced by glutamic acid to mimic constitutive phosphorylation

Table 2. Peptides identified on purified Lgd protein

| Peptide sequence | Mascot score | Q value | Binomial peptide score | Best site probability | PSM modification position in protein | Mascot score control |
|---|--------------|---------|------------------------|-----------------------|--------------------------------------|----------------------|
| K. SINVDIPPEVSVKPIGGQAPPVPAEESPAP STPASPPVPSR. A | 38 | 0 | 58 | S36(P):89.57 | 1×Phospho [S225(89.6)] | 51 |
| R. AAPDPPTGTPVEPTTSVAPTSPPNPLVTQMR. S | 48 | 0 | 128 | T10 (P): 96.47 | 1×Phospho [T242(96.5)] | 13 |
| R. AAPDPPTGTPVEPTTSVAPTSPPNPLVTQMR. S | 48 | 0 | 113 | T7 (P): 96.82 | 1×Phospho [T239 (96.8)] | 13 |
| K. MQEEAAAEVAEPTAAPEPTPVAPVLAATNMLEALQQR. L | 65 | 0 | - | T20 (P) | 1×Phospho [T347] | - |

Lgd is phosphorylated *in vitro* by CycB/Cdk1. Mass spectrometry was performed on purified Lgd protein treated with CycB/Cdk1 and 200 μ M of ATP, and on purified Lgd protein plus 200 μ M of ATP but without CycB/Cdk1 (control). A list of peptides detected and their phosphorylation is indicated, with their Mascot score, Q-value, binomial peptide score, best site probability, PSM modification position in protein and Mascot score for the control provided by the Proteome Discoverer 2.1 program. Analysis detected phosphorylation modifications at positions S225, T239, T242 and T347 (red stars in Fig. 2B).

(Fig. 3A). The wild-type variant appeared more stable than the mutant variants, and was expressed at a much lower level relative to endogenous Lgd (Fig. S3A).

GSC abscission starts with the formation of a transient ring canal (RC), which later constricts as a midbody (MB) visualized by a bulge of fusome. Wild-type Lgd was detected at the GSC/CB midbody (Fig. 3B,F), but never at the earlier RC (Fig. S3B). Both Lgd14A and Lgd5A showed the same pattern as the wild type form (Fig. 3C,D,F and Fig. S3C,D). In contrast, Lgd5E was mostly cytoplasmic and barely detectable at the midbody (Fig. 3D,F and Fig. S3E). These observations showed that Lgd accumulates to the intercellular bridge only at the late stages of abscission (MB stage), and that this localization does not require phosphorylation at Cdk1 sites. Indeed, phosphorylation of Lgd could instead prevent its localization at the midbody, as Lgd5E was found to be mostly cytoplasmic.

Lgd phosphorylation potentiates Shrub activity during GSC abscission

We thus investigated the functional relevance of Lgd phosphorylation during GSC abscission by testing whether the transgenes LgdWT, Lgd14A, Lgd5A and Lgd5E were able to compensate for the complete absence of Lgd in germline clones homozygous mutant for *lgd*^{d7}. One copy of Lgd-WT was sufficient to fully rescue GSC abscission defects, as we did not detect any stem-cysts (Fig. 4A,B). We also found that all three variants, Lgd14A, Lgd5A and Lgd5E, were able to rescue most of GSC abscission, although a few stem-cysts still formed (Fig. 4A,B, Fig. S4A). These results indicated that Lgd phosphorylation by Cdk1 is not essential for proper GSC abscission. Nevertheless, the presence of few stem-cysts in all three variants suggested that abscission was not efficient under these conditions. To test this possibility, we used a sensitized genetic background in which GSC abscission is delayed. We previously showed that GSC abscission is very sensitive to *shrub* gene dosage (Matias et al., 2015). Indeed, 84% of germaria heterozygous for *shrub* (*shrub*^{+/+}) formed stem-cysts (Fig. 4C). We found that adding one copy of the LgdWT transgene was sufficient to significantly reduce the number of stem-cysts in *shrub*^{+/+} germaria (Fig. 4C). A similar rescue was observed with Lgd5E (Fig. 4C). In contrast, neither Lgd14A nor Lgd5A was able to compensate for the absence of one copy of *shrub* (Fig. 4C). We further showed that this absence of rescue is not caused by the inability of Lgd14A to bind Shrub (Fig. S4B). Altogether, these results revealed that LgdWT was able to potentiate the activity of the remaining Shrub in *shrub* heterozygous GSC. In addition, it showed that Lgd phosphorylation was required for this positive effect.

To better understand how the phosphorylation of Lgd affects ESCRT-III localization in this sensitized *shrub*^{+/+} background, we quantified the levels of CHMP2B at the intercellular bridge of GSCs at different stages of cytokinesis. We found that in a *shrub*^{+/+} background, the levels of CHMP2B-GFP are dramatically reduced at all stages of abscission (Fig. 4D,E, Fig. S4C), in agreement with recent findings (Pfitzner et al., 2020). In addition, we found that all three forms of Lgd (WT, 5A and 5E) were able to partially rescue the levels of CHMP2B during the early stages of cytokinesis (P+B and F stages). However, only Lgd-WT and Lgd-5E rescued a strong accumulation of CHMP2B at the midbody during the late stages of abscission. Although Lgd-5A was able to increase CHMP2B levels, it was significantly less potent than Lgd-WT (Fig. 4E). These results suggested that, in late cytokinesis, increased phosphorylated Lgd levels promote the strong enrichment of ESCRT-III that is necessary for abscission.

DISCUSSION

In this work, we show that, during *Drosophila* GSC abscission, ALiX and Lgd act redundantly for the proper localization of ESCRT-III proteins at the abscission site. In *alix* mutant GSCs, the amount of CHMP2B at the ring canal was reduced compared with wild type, and removing Lgd in this context further decreased CHMP2B levels at the intercellular bridge. These results showed that both ALiX and Lgd play a positive role in the localization of ESCRT-III proteins. Because 30% of GSCs still exhibited some Shrub-HA staining at the intercellular bridge in absence of both Alix and Lgd, other pathways, such as the ESCRT-I-ESCRT-II-CHMP6 pathway (Christ et al., 2016), or the lipid kinase PI3K-C2 α with ESCRT-II (Gulluni et al., 2021) may additionally be involved in Shrub recruitment. However, Alix and Lgd appear to be major regulators, as 70% of GSCs are completely devoid of Shrub-HA. In agreement, removing one copy of *alix* enhanced the abscission phenotypes in GSCs lacking *lgd*. By contrast, in *lgd* single mutants, we measured increased amounts of CHMP2B at the ring canal, indicating that Lgd also plays a negative role in localizing ESCRT-III at the ring canal. In such a role, Lgd could participate in the removal of ESCRT-III subunits necessary for the dynamic formation of ESCRT-III polymers or sequester ESCRT-III in the cytoplasm.

We also found that Lgd is phosphorylated by Cdk1 *in vitro* and *in vivo*. We propose that phosphorylation of Lgd could impact its activity on ESCRT-III. Although we found that all variants of Lgd (Lgd14A, Lgd5A and Lgd5E) were able to rescue the absence of *lgd* in the majority of GSCs abscission, only the wild-type form is able to fully rescue GSC abscission (Fig. 3B). It indicated to us that when Lgd phosphorylation sites are mutated (non-phosphorylatable or phosphomimic), abscission is not as robust as in wild-type conditions. As Shrub is a target of Lgd, and is haplo-insufficient, we reasoned that removing one copy of *shrub* (*shrub*^{+/+}) could provide a sensitized genetic background to reveal a stronger requirement for Lgd phosphorylation sites. Indeed, we found that, although the phosphomimic Lgd5E and LgdWT were able to rescue the abscission phenotype of decreased Shrub levels (*shrub*^{+/+}), the non-phosphorylatable forms Lgd14A and Lgd5A were unable to rescue, suggesting that the phosphorylated form of Lgd have a positive effect on ESCRT-III-mediated abscission. Consistently, Lgd5E and LgdWT were both able to promote strong CHMP2B-GFP enrichment at the abscission site at late stages of abscission, whereas Lgd5A was less potent. The role of Lgd on ESCRT-III localization could thus depend on the relative levels of phosphorylated and non-phosphorylated forms of Lgd.

Cytokinesis of *Drosophila* GSC is a long process, where the two daughter cells remain connected by a ring canal until the G2 phase of the next cell cycle. The ring canal then constricts into a midbody, and abscission occurs after 11 h (de Cuevas and Spradling, 1998; Matias et al., 2015; Villa-Fombuena et al., 2021). During this period, Cyclin/Cdk1 activity increases and Cyclin B localizes at the midbody of *Drosophila* GSCs and of vertebrate HeLa cells (Mathieu et al., 2013). Furthermore, inhibiting Cdk1 activity delays abscission in both systems, which demonstrates a positive role for Cdk1 in abscission (Mathieu et al., 2013). Here, our biochemical results demonstrate that Cdk1 can directly phosphorylate Lgd. We propose that Cdk1 could regulate the relative amounts of phosphorylated and non-phosphorylated forms of Lgd differentially from early to late abscission stages (from ring canal to midbody stage). In our model (Fig. S4D), non-phosphorylated Lgd could bind Shrub and bring it to the abscission site, where Shrub could be anchored by ALiX at the abscission site. The phosphorylation of Lgd by Cdk1 at the midbody would allow the release of Shrub from Lgd and its transfer to ALiX at

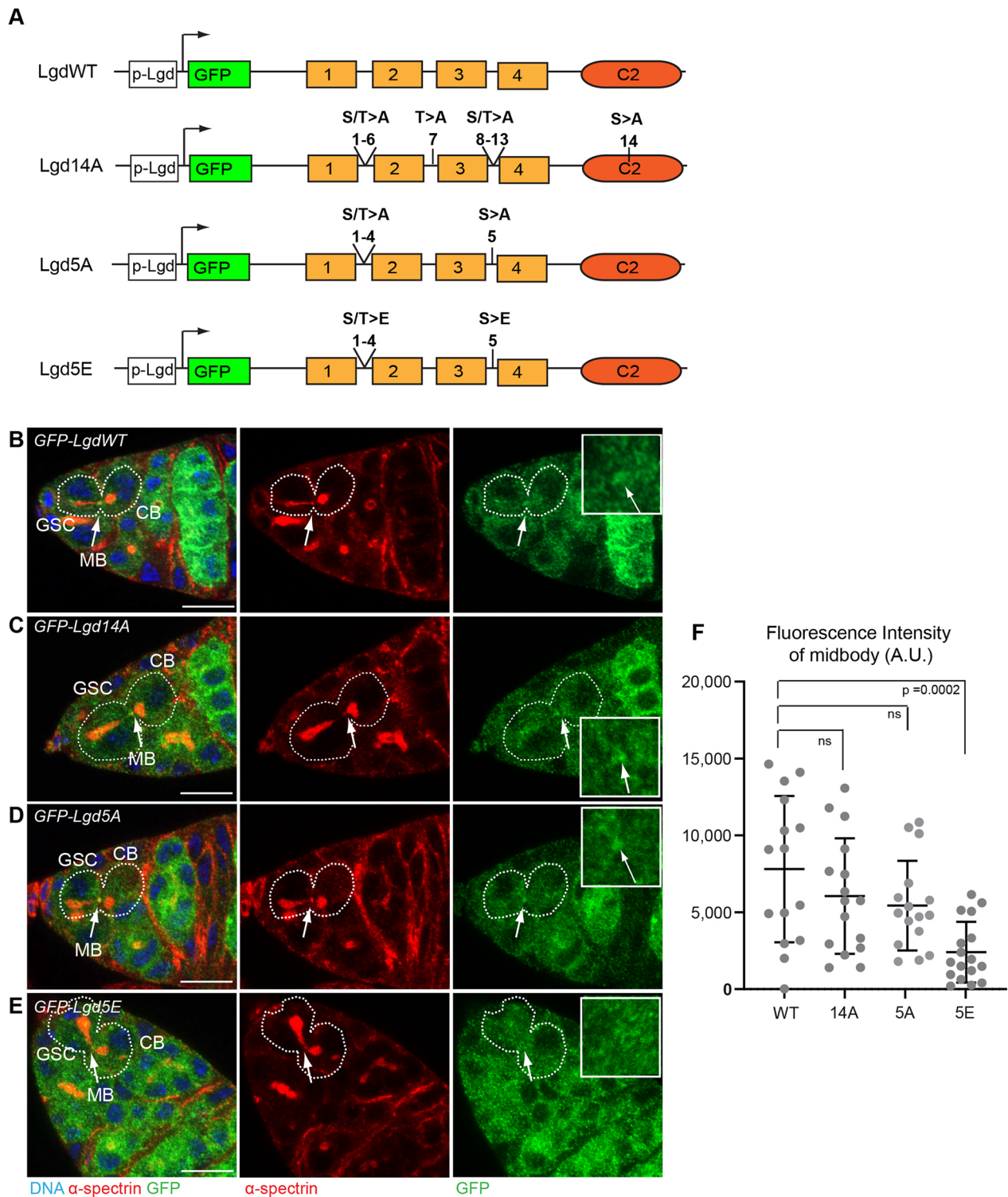


Fig. 3. Lgd phosphorylation by Cdk1 is not necessary for its midbody localization. (A) Schematic of the four GFP-Lgd variants generated for this study. All transgenes were inserted at the same genomic locus: attP154. All Lgd variants were expressed under the control of Lgd promoter (p-Lgd) and Lgd-coding sequence was fused to GFP at its N-terminal part. In Lgd14A, all the Cdk1 consensus sites were mutated into alanine (A) (S217A, T222A, S225A, T239A, T242A, S254A, T347A, T436A, S442A, S445A, T457A, T465A, S474A and T712A) to generate a non phosphorylatable Lgd variant. In Lgd5A and Lgd5E, only the five phosphorylation sites identified by mass spectrometry in *Drosophila* embryos (S225, T239, T242, S254 and S474) were mutated, either into alanine or glutamic acid (E, to form a phospho-mimetic form). (B-E) Confocal images of germaria obtained from females expressing the four GFP-Lgd variants immunostained for α -spectrin (red) and GFP (green). Dashed lines surround GSC/CB pairs. White arrows indicate midbodies. Insets on the right show midbody areas at higher magnification. Scale bars: 10 μ m. (F) Fluorescence intensity quantified at the midbody on the y-axis (arbitrary unit, A.U.), GFP-Lgd variants on the x-axis: GFP-lgd-WT (WT, $n=14$), GFP-lgd-14A (14A, $n=15$), GFP-lgd-5A (5A, $n=15$) and GFP-lgd-5E (5E, $n=16$). Data are mean \pm s.e.m. unpaired *t*-tests were carried out and *P*-values are indicated. ns, non-significant.

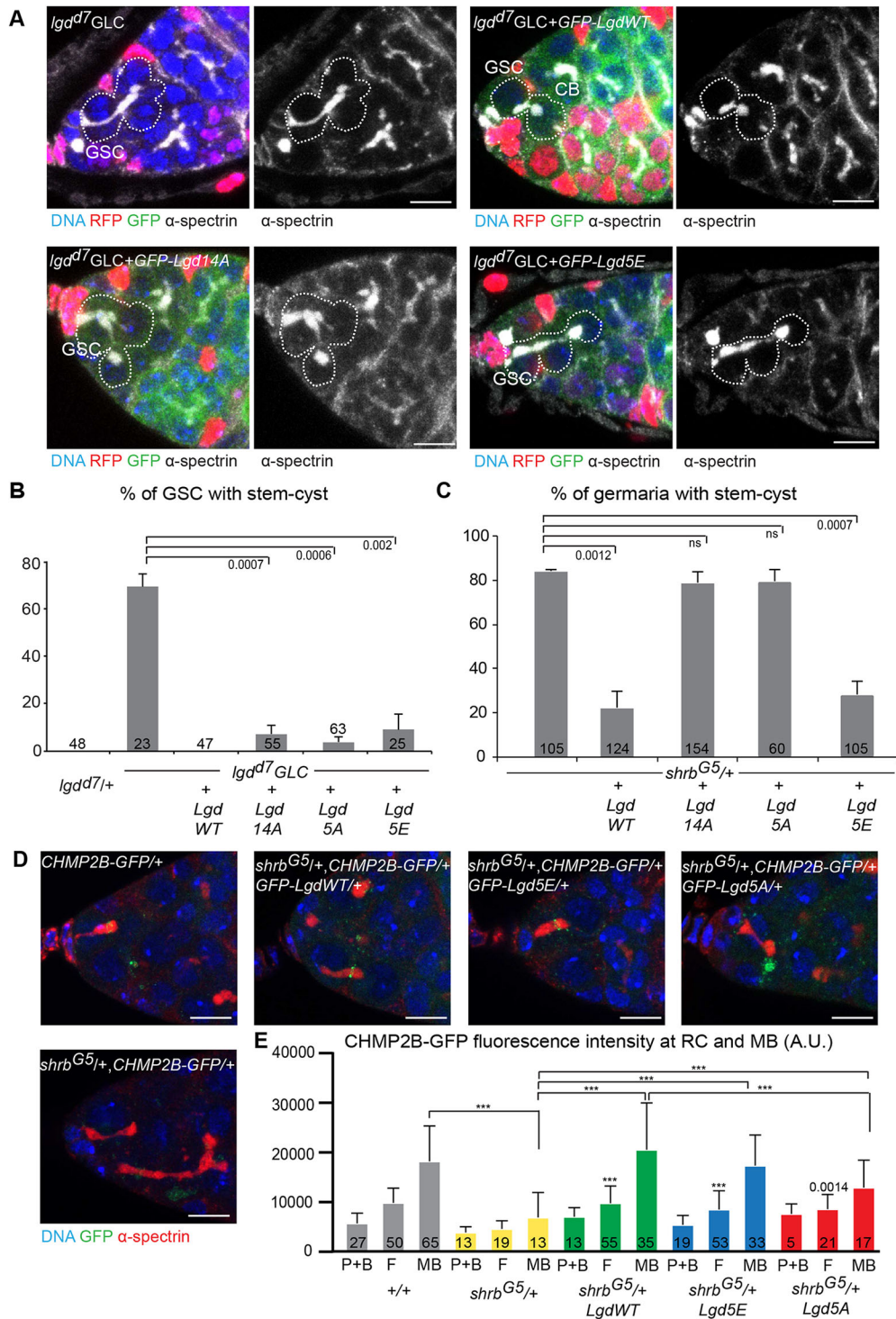


Fig. 4. Phosphorylation of Lgd is required for abscission when Shrub levels are reduced. (A) Confocal images of germaria obtained from females with *Igd^{d7}* GLC (RFP-negative cells) expressing or not each of the four GFP-Lgd variants immunostained for α -spectrin (white) and GFP (green). Dashed lines surround GSC/CB pairs (*Igd^{d7}*GLC+*Lgd*WT) or stem-cysts (*Igd^{d7}* GLC, *Igd^{d7}* GLC+*Lgd*14A, *Igd^{d7}* GLC+*Lgd*5E). The anterior-most GSC is indicated. Scale bars: 10 μ m. (B) Percentage of GSCs exhibiting a stem-cyst phenotype (*y*-axis). Genotypes are on the *x*-axis. Unpaired *t*-tests were used to compare *Igd^{d7}* GLC and *Igd^{d7}* GLC plus *Lgd* variants. Data are mean \pm s.e.m. of three experiments; *P*-values are derived from an unpaired *t*-test and are indicated. Numbers of GSCs analyzed are indicated. (C) Percentage of germaria exhibiting at least one stem-cyst (*y*-axis). Genotypes are on the *x*-axis. Data are mean \pm s.e.m. of three experiments, *P*-values are derived from an unpaired *t*-test and are indicated; ns, non-significant. Numbers of germaria analyzed are indicated. (D) Confocal images of germaria obtained from wild-type or *shrb^{G5}/+* females expressing CHMP2B-GFP and/or each of the Lgd variants immunostained for α -spectrin (red). The GSC/CB pairs are at the fusing stage. Scale bars: 10 μ m. (E) Fluorescence intensity (arbitrary unit, A.U.) of CHMP2B-GFP at the ring canal of a GSC [at Plug+Bar (P+B) or fusing (F) stages] or at the midbody (MB) of a GSC in control (grey), *shrb^{G5}/+* (yellow), *shrb^{G5}/+*, *Lgd*WT/+ (green), *shrb^{G5}/+*, *Lgd*5E/+ (blue) and *shrb^{G5}/+*, *Lgd*5A/+ (red) ovaries. Numbers of GSCs analyzed are indicated. *P*-values are derived from Wilcoxon-Mann-Whitney tests. *P* values of comparisons made at the MB stage are indicated at the top of the graph. Comparisons made at the fusing stage were between *shrb^{G5}/+* and *shrb^{G5}/+* plus Lgd variants, and are indicated above the quantification bars of the variants. ****P*<0.0001.

the midbody, whereas phosphorylated Lgd would remain in the cytoplasm. This phosphorylation event could either decrease Lgd affinity for Shrub or decrease Lgd stability as we showed that Lgd-5E appears less stable than LgdWT (Fig. S3A). This model would also explain why Lgd-5E is not detected at the mature midbody. Phosphorylated Lgd would thus be able to transfer Shrub to ALiX, and would then play a positive role in Shrub accumulation and abscission completion, whereas non-phosphorylated Lgd would remain bound to Shrub, inhibiting its binding to ALiX and its accumulation at the midbody. We conclude that Lgd phosphorylation is required to fine-tune the recruitment and dynamics of ESCRT-III for a robust abscission timing.

Further work should decipher whether Lgd phosphorylation is strictly necessary for other ESCRT-dependent membrane remodeling processes. For example, cell-cycle regulated processes, such as the resealing of the nuclear envelope could be critically regulated by the levels of phosphorylated Lgd. During this process, phosphorylated Lgd could negatively regulate CHMP4 as it does during abscission. In addition, Lgd localization during nuclear envelope resealing depends on its binding to CHMP7 (Ventimiglia et al., 2018). This binding may be regulated in time by the phosphorylation of Lgd. It would also be interesting to investigate whether other membrane remodeling events relying on ESCRT function, such as viral budding, exosome release, membrane repair or autophagy, are regulated directly by the cell cycle machinery or indirectly through the Cdk1-dependent phosphorylation of Lgd.

MATERIALS AND METHODS

Fly stocks and genetics

Fly stocks were grown under standard conditions. The food was made of agar (75 g), wheat flour (350 g), dry backer yeast (500 g), sugar (550 g) and water (10 liters). 25 g methyl 4-hydroxybenzoate in 250 ml ethanol and 40 ml propionic acid were added to the food before filling the tubes. *Drosophila* alleles used in this study were: *nos-GAL4* (Van Doren et al., 1998), *shrb^{G5}* (Vaccari et al., 2009), *alix³* (Eikenes et al., 2015), and *lgd^{d7}* (Buratovich and Bryant, 1997). The transgenes used were *CHMP2B-GFP* (PBac{fTRG00825.sfGFP-TVPTBF}/VK00002/VDRCv318679), which allows expression of CHMP2B under its endogenous regulatory sequences (Sarov et al., 2016), TRIP lines allowing shRNA expression (Ni et al., 2011) directed against *white* (P{TriP.GL00094}attP2 / BL35573) as a control or *lgd* (this study), and UASp-shrb-HA (Mathieu et al., 2022). Recombinants were obtained using standard genetic procedures.

Overexpression experiments were performed using the GAL4/UASp system (Brand and Perrimon, 1993) with the *nanos-GAL4-VP16* driver. Germline clones were generated using the FLP/FRT technique (Chou and Perrimon, 1992) using *hsFLP* and a *H2B-RFP* transgene recombined onto *FRT40A*. Clones were induced by heat-shocking second or third instar larvae at 37°C for 2 h, females were dissected 1-2 days after eclosion.

Cell culture, transfection and drug treatments

Drosophila S2 cells (Thermo Fisher Scientific) were cultured at 25°C in Schneider's *Drosophila* medium (Thermo Fisher Scientific) supplemented with 10% FBS plus 1% streptomycin/penicillin. Transfection of *Drosophila* S2 cells was performed using Effectene transfection Reagent (Qiagen) according to the manufacturer's instruction. Cells were transfected with 1 µg of DNA for 48 h before immunoprecipitation. Cells were treated with 20, 50 or 100 µM of RO3306 (Sigma Aldrich) or DMSO (Sigma Aldrich) for 12 h before immunoprecipitation.

Immunostainings on ovaries

Antibodies and Hoechst staining were performed according to standard protocols. Briefly, ovaries were dissected in PBS, fixed in 4% PFA for 20 min, permeabilized in PBT (PBS-0.2% Triton) for 30 min, left overnight with primary antibodies in PBT at 4°C, washed three times for 15 min in

PBT, left with secondary antibodies for 2 h at room temperature, washed 1 h in PBT and mounted in Cityfluor.

The primary antibodies used in this study were as follows: mouse-anti- α -Spectrin (clone 3A9, DSHB, 1:500), rabbit anti- α -Spectrin (1:1000; Byers et al., 1987), rabbit anti-GFP (50430-2-AP, Proteintech, 1:500) and rabbit anti-HA (Cell Signaling Technologies, C29F4, 1:200). Fluorescent secondary antibodies were from Jackson ImmunoResearch; Hoechst was from Molecular Probes.

Molecular biology: constructs for transgenic flies

To generate pCASPER4-pUASp-GFP-Lgd-attB, the whole-length Lgd cDNA was amplified by PCR from *lgd* cDNA clone (LD23056) plasmid, using the primers 5'GGGGACAAGTTTGTACAAAAAAGCAGGCTCATGTTCTCCAGAAAGAAGCCAGAGCCA3' and 5'GGGGACCAC-TTTGTACAAGAAAGCTGGGTCTAGGCATCCAAGACCAACCACT-TTTC3', and inserted into pDONR201. The *lgd* cDNA was then transferred by LR recombination to pPGW destination vector (obtained from Terence Murphy's laboratory Drosophila Gateway Vector Collection) to generate a pCASPER4-pUASp-GFP-Lgd vector. Finally, a PCR fragment of the UASp-GFP-Lgd sequence was amplified on pUASp-GFP-Lgd vector using the primers 5'CTTCGTATAATGTATGCTATACGAAGTTATGCTAGC-GGATCCCTGGTACATCAAATACCTTGGATC3' and 5'TCGTCGACACTAGTTCTAGAGGTACCCTCGAGCCGCGCCGATTAACCT-TAGCATGTCCTGGGG3', and inserted by SLIC reaction into the pCasper4-pUbi-attB vector digested by NotI and BamHI (which removes the pUbi promoter) to generate pCASPER4-pUASp-GFP-Lgd-attB. Transgenic lines were then generated by injection into y1 w67c23; P{CaryP}attP2 flies by BestGene Inc.

To generate the plasmids pCASPER4-pUASp-GFP-Lgd14A-attB and pCASPER4-pUASp-GFP-Lgd14E-attB, point mutations were introduced into the Lgd sequence in several steps. First, two fragments encoding mutated Lgd CDS using StuI-S217A/E, T222A/E, S225A/E, T239A/E, T242A/E, S254A/E-EcoRI (fragment 1) and EcoRI-T347A/E, T436A/E, S442A/E, S445A/E, T457A/E, T465A/E, S474A/E-HpaI (fragment 2) were produced by Eurofin. They were then amplified by PCR using the following primers: 5'CCAAGACTGCCGCGATTCTGGCAAAGCAAGGCGAT-TTGAAGAGGCCCTAAGACTCTGAAAGATCTG3' and 5'GCGACA-GCTTCTGCGGCTGCTTCTTCTTGCATTTTTTAAAGGAATTAAGA-AACTCAGCTGGTGGAG3' for fragment 1, and 5'GTTGATTTGAGT-GACATGCCCTCCACCAGCTGAGTTTCTTGAATTCCTTAAAAA-AATGCAAGAAG3' and 5'CGGCAATATTATTCTTCTGCTGATTGC-CAGACGTGCGTGTGTTAACTCTTTGGGCTTAGGAGGTG3' for fragment 2. PCR fragments were then inserted by ligation into Lgd cDNA clone LD23056 digested by StuI and HpaI. Next, S474A/E point mutations were generated by GeneTailor Site-Directed Mutagenesis system with the primers 5'ATGTTATCAGAGACACCAGCGCTCCTGACTACGA3' and 5'GCTGGTGTCTCTGATAACATTGGTTTTAGT3' for S474A or with 5'ATGTTATCAGAGACACCAGCGAACCTGACTACGA3' and 5'GC-TGGTGTCTCTGATAACATTGGTTTTAGT3' for S474E. Finally, the mutated Lgd CDS were transferred by Gateway cloning into pPGW to add the UASp promoter and N-terminus GFP, and finally into the pCasper4-attB-pUbi vector digested by NotI and BamHI (which removes the pUbi) to generate pCASPER4-pUASp-GFP-Lgd14A-attB and pCASPER4-pUASp-GFP-Lgd14E-attB vectors. Transgenic lines were generated by injection into y1 w67c23; P{CaryP}attP2 flies by BestGene Inc.

To generate the plasmid pCASPER4-plgd-GFP-Lgd-attB, we amplified *lgd* promoter region (419pb in 5') and 3'UTR (416pb) on genomic DNA using the following primers: 5'GCATGTCGATCCGCTAGCGCTG-TACCGGTTATCGATTTCGATTAGACAGC3' and 5'GGTGAACAGCTC-CTCGCCCTTGTCTACCATCCTTGATTGCACAGAGGCTG3' for the promoter and 5'TGGTTGGTCTTGGATGCCTGAAGATCTCCATAGG-GCTAAACAAGAAAATTTAAATAAATAG3' and 5'TTTTATTAAC-TACATACATACTAGAATTCGGAGTTGTAGTTCAACAAAC3' for the 3'UTR.

The GFP-Lgd sequence was amplified from pCASPER4-pUASp-GFP-Lgd with the primers 5'CAGCCTCTGTGCAATCAAGGATGGTGAG-CAAGGGCGAGGA3' and 5'CTATTTTATTTAAATTTCTTGTGTTAG-CCCTATGGAGATCTTCAGGCATCCAAGACCAACCA3'. All three

fragments were then inserted into pCASPER4-AttB digested using EcoRI and AgeI. Transgenic lines were generated by injection into y1 w67c23; P{CaryP}attP154 flies by BestGene Inc.

To generate pCASPER4-plgd-GFP-Lgd14A-AttB, we used the same strategy as for pCASPER4-plgd-GFP-Lgd-AttB but we used pCASPER4-pUASp-GFP-Lgd14A to amplify the GFP-Lgd14A fragment. Transgenic lines were generated by injection into y1 w67c23; P{CaryP}attP154 flies by BestGene Inc.

To generate the intermediate plasmid pBluntII-GFP-Lgd, we amplified a fragment of PCR from pCASPER4-plgd-GFP-Lgd-AttB encompassing lgd promoter, lgd CDS and lgd 3'UTR with the primers 5'GCATGTCGATCCGCTAGCGCTGTACCGTTATCGATTTCGATTAGACAGC3' and 5'TTTTATTAACCTACATACATACTAGAATTCGGAGTTGTAGT-TCAACAAAC3', and cloned it into pCR-BluntII-TOPO (ThermoFisher).

To generate the plasmid pCASPER4-plgd-GFP-Lgd5A-AttB, S225A, T239A, T242A, S254A, S474A non-phosphorylatable point mutations in the Lgd-coding sequence were generated by GeneTailor Site-Directed Mutagenesis System on the plasmid pBluntII-GFP-Lgd using the following primers pairs: 5'CTCCTTCCACACCTGCTGCTCCTCCGCTG3' and 5'AGCAGGTGTGGAAGGAGCTGGTACTC3' for S225A; 5'GCTCCAGATCCACAGCTCCCGCTCCCGTGGAGC3' and 5'TGGTGGATCTGGAGCTGCACGACTAG3' for T239 and T242A; 5'CATCTGTG-GCTCCCACAGCTCCCCCTAATC3' and 5'CATCTGTGGCTCCCAC-AGCTCCCCCTAATC3' for S254A; 5'CTCCTCGAAAAGCACCTGCT-CCTCCTAAGC3' and 5'AGGTGCTTTTCGAGGAGCTGTAGGTGTC3' for S474A to generate a pBluntII-GFP-Lgd5A.

plgd-GFP-Lgd5A sequence was then amplified with the primers 5'GCATGTCGATCCGCTAGCGCTGTACCGTTATCGATTTCGATTAG-ACAGC3' and 5'TTTTATTAACCTACATACATACTAGAATTCGGAG-TTGTAGTTCAACAAAC3' and inserted by SLIC into pCASPER4-AttB digested using EcoRI and AgeI. Transgenic lines were generated by injection into y1 w67c23; P{CaryP}attP154 flies by BestGene Inc.

To generate the plasmid pCASPER4-plgd-GFP-Lgd5E-AttB, S225E, T239E, T242E, S254E, S474E phosphomimetic point mutation in the Lgd-coding sequence were generated by GeneTailor Site-Directed Mutagenesis System on the plasmid pBluntII-GFP-Lgd using the following primers: 5'CTCCTTCCACACCTGCTGAACCTCCGCTG 3' and 5'AGCAGGTGTGGAAGGAGCTGGTACTC3' for S225E; 5'GCTCCAGATCCAC-CAGAACCCGCGCAACCCGTGGAGC3' and 5'TGGTGGATCTGGAG-GCTGCACGACTAG3' for T239E and T242E; 5'CATCTGTGGCTCC-CACAGAACCCCTAATC3' and 5'TGTGGGAGCCACAGATGTAG-TGGGCTC3' for S254E; and 5'CTCCTCGAAAAGCACCTGAACCTCC-TAAGC3' and 5'AGGTGCTTTTCGAGGAGCTGTAGGTGTCG3' for S474E to generate a pBluntII-GFP-Lgd5E. The plgd-GFP-Lgd5E sequence was then amplified with the primers 5'GCATGTCGATCCGCTAGCG-CCTGTACCGTTATCGATTTCGATTAGACAGC 3' and 5' TTTTATTA-ACCTACATACATACTAGAATTCGGAGTTGTAGTTCAACAAAC 3', and inserted by SLIC into pCASPER4-AttB digested using EcoRI and AgeI. Transgenic lines were generated by injection into y1 w67c23; P{CaryP}attP154 flies by BestGene Inc.

To generate the sh-RNA-Lgd, the primers 5'CTAGCAGTCTGC-AGCAACGTTTAGAGAAAATAGTTATATTCAAGCATATTTCTCTAAA-CGTTGCTGCAGGCG3' and 5'AATTCGCCTGCAGCAACGTTTAGA-GAAATATGCTTGAATATAACTATTCTCTAAACGTTGCTGCAGA-CTG3' were annealed and ligated into the Valium 22 plasmid. Transgenic lines were generated by injection into y, v; attP2 flies by Genetic Services. The line is homozygous viable.

Molecular biology: constructs for S2 cells transformations

To generate the intermediate plasmid pCASPER4-pUbi-HA-AttB, we annealed the primers 5'GATCCACTAGTGGCCTATGCGGCCGATG-TACCCATACGATGTTCCAGATTACGCTTAAG3' and 5'CCTAGGTG-GAGATCTTTTAGTACCTTAAGCGTAATCTGGAACATCGTATGG-GTACATGC3' (to obtain HA fragment) and inserted them by SLIC into pCASPER4-pUbi-attB digested by NotI and KpnI.

To generate the pCASPER4-pUbi-Nter-Lgd-HA-attB, a PCR fragment corresponding to domain DM14 1 and 2 was amplified from plasmid pBluntII-GFP-Lgd using the primers 5'CTAGTGGCCTATGCGGCCG

ATGTTCTCCAGAAAGAAGCC3' and 5'GGAACATCGTATGGGTA-CATAAGGAATTCAAGAAACTAG3', and inserted into pCASPER4-HA-AttB digested by NotI.

To generate the plasmids pCASPER4-pUbi-GFP-Lgd-AttB, pCASPER4-pUbi-GFP-Lgd14A-AttB and pCASPER4-pUbi-GFP-Lgd14E-AttB, the CDSs of GFP-Lgd, GFP-Lgd14A and GFP-lgd14E were amplified by PCR on the plasmids pCASPER4-pUASp-GFP-Lgd, pCASPER4-pUASp-GFP-Lgd14A and pCASPER4-pUASp-GFP-Lgd14E, respectively, with the Gprimers 5'CTAGTGGCCTATGCGGCCGATGGTGAGCAAGGGCG-AGGA3' and 5'GGTTGGTCTTGGATGCCTGAAGATCTCCACCTAG-GTGACG3'. The PCR products were inserted into pCASPER4-pUbi-attB digested using BglII and NotI.

Biochemistry

GFP immunoprecipitation on embryos and ovaries

GFP immunoprecipitation (IP) experiments were performed using 25 μ l of magnetic GFPTrap R-M beads (Chromotek) per experimental condition. Beads were first equilibrated by three washes in washing buffer [50 mM Tris (pH 7.4), 150 mM NaCl, 1 mM EDTA (pH 8), 1 \times Complete EDTA-free Protease inhibitor cocktail (Roche) and 2 \times PhosSTOP Phosphatase inhibitor cocktail (Roche)]. For mass spectrometry analysis, 0 h- to 12 h-old embryos expressing pUAS-GFP-lgd-WT under the control of *nos-GAL4* were bleach dechorionated and lysed in lysis buffer [50 mM Tris (pH 7.4), 150 mM NaCl, 0.1% NP40, 1 mM EDTA (pH 8), 1 mM DTT, 1 \times Complete EDTA-free Protease inhibitor cocktail (Roche) and 2 \times PhosSTOP Phosphatase inhibitor cocktail (Roche)] for 30 min at 4°C under rotation at 30 rpm. Homogenates were clarified via two rounds of microfuge centrifugation for 15 min at 4°C, and then incubated with washed magnetic GFPTrap R-M beads (Chromotek) under rotation at 15 rpm at room temperature for 1 h. After magnetic separation, the beads were washed twice with washing buffer, resuspended in 4 μ l of H₂O and sent to a mass spectrometry platform (Institut Jacques Monod-Université Diderot). The samples were treated with trypsin and the raw data analyzed with Proteom Discoverer 2. Alternatively, 100 ovaries expressing pUAS-GFP-lgd-WT under the control of *nos-GAL4* were dissected in Schneider medium and subjected to the same lysis and immunoprecipitation protocol.

HA-immunoprecipitation on S2 cells followed by λ -phosphatase treatment

HA-immunoprecipitation (IP) experiments were performed with 25 μ l of Pierce Anti-HA Magnetic Beads (Thermo Fisher). Beads were first equilibrated by three washes in washing buffer [50 mM Tris (pH 7.4), 150 mM NaCl, 1 mM EDTA (pH 8), 10% glycerol, 1 \times Complete EDTA-free Protease inhibitor cocktail (Roche) and 2 \times PhosSTOP Phosphatase inhibitor cocktail (Roche)]. Pellets of S2 cells were lysed in 1 ml of lysis buffer [50 mM Tris (pH 7.4), 150 mM NaCl, 0.1% NP40, 1 mM EDTA (pH 8), 10% glycerol, 1 \times Complete EDTA-free Protease inhibitor cocktail (Roche) and 2 \times PhosSTOP Phosphatase inhibitor cocktail (Roche)] for 30 min at 4°C under rotation at 30 rpm. Homogenates were clarified via two rounds of microfuge centrifugation at 16,000 g for 15 min at 4°C and then \sim 1 ml incubated with washed Pierce Anti-HA Magnetic Beads under rotation at 15 rpm at room temperature for 1 h. 75 μ l of homogenates were added to 25 μ l of Laemmli buffer (4 \times) and denatured at 95°C for 10 min to get the Input. After magnetic separation, the pellets were washed twice in washing buffer, then divided in two and incubated in 50 μ l of either solution A [condition without λ -phosphatase: 10 \times buffer for PMP (Biolabs), 10 mM MnCl₂, 1 \times Complete EDTA-free Protease inhibitor cocktail (Roche) and 2 \times PhosSTOP Phosphatase inhibitor cocktail (Roche)] or 50 μ l of solution B [condition with 0.5 μ l of λ -protein-phosphatase (Biolabs): 10 \times buffer for PMP (Biolabs), 10 mM MnCl₂ and 1 \times Complete EDTA-free Protease inhibitor cocktail (Roche)] for 30 min at 30°C. Pellets were then resuspended in 50 μ l of Laemmli buffer (4 \times) and denatured at 95°C for 10 min; finally bound proteins were recovered from the beads by magnetic separation. For western blotting, 10 μ l of these HA-IP enriched proteins and Input were fractionated on 4-15% gradient mini-protean TGX precast gels (Bio-Rad) at 140 V for 2 h in ice and transferred using Tans-Blot Turbo mini nitrocellulose transfer packs (Bio-Rad).

HA co-immunoprecipitation in S2 cells

To immunoprecipitate HA-tagged Shrub protein, pellets of S2 cells were lysed in 1 ml of lysis buffer [50 mM Tris (pH 7.4), 150 mM NaCl, 0.1% NP40, 1 mM EDTA (pH 8), 10% glycerol and 1×Complete EDTA-free Protease inhibitor cocktail (Roche)] for 30 min at 4°C under rotation at 30 rpm. Homogenates were clarified via two rounds of microfuge centrifugation for 15 min at 4°C and the supernatant recovered. 50 µl was kept and diluted with 2×Laemli as Input (1/20 of total). The rest was then incubated with 25 µl of pre-washed Pierce Anti-HA Magnetic Beads (Thermo Fisher) under rotation at 15 rpm at room temperature for 1 h. Beads were then washed twice with washing buffer [50 mM Tris (pH 7.5), 150 mM NaCl, 10% glycerol, 1 mM EDTA (pH 8) and 1×Complete EDTA-free Protease inhibitor cocktail]. The pellets were then resuspended in 100 µl of 1×Laemmli in 0.5×washing buffer and denatured at 95°C for 10 min; bound proteins were recovered from the beads by magnetic separation and analyzed by western blots. Samples (same volume of IP and of input) were loaded on Bio-Rad precast gels (Mini-PROTEAN TGX, 456-1095) and transferred onto nitrocellulose membranes (Bio-Rad Trans-Blot Turbo Transfer Pack, 1704158).

Primary antibodies used after immunoprecipitations were rabbit anti-HA (Sigma, H6908, 1:1000), mouse-anti-tubulin DM1A (T902, Sigma Aldrich, 1:5000) and rabbit-anti-GFP (Institut Curie, proteomic platform, 1:10,000). Secondary antibodies were from Jackson ImmunoResearch. Bands were detected with the ECL Prime Western Blotting Detection Reagents (GE Healthcare) and visualized using a mini-LAS-4000 Imaging System (Fujifilm).

Lgd-His protein production

We used the Bac-to-Bac Baculovirus Expression System (Invitrogen). We first amplified a fragment of Lgd CDS on Lgd cDNA clone LD23056 with the primers 5'CCGAAAACCTGTATTTTCAGGGCGCCATGGATCCG-GAATTCTTCTCCAGAAAGAAGCCAGAGC3' and 5'CTTCTCGACA-AGCTTGGTACCGCATGCCTCGAGACTGCAGCTAGGCATCCAAGACCAACCAC3' and inserted the PCR product into pFastBAC-HTA donor plasmid digested by EcoRI and PstI to obtain pFastBac-HTA-Lgd. After transformation into MAX Efficiency DH10Bac cell, Recombinant Bacmid DNA was obtained and used to transfect SF9 cells to produce Baculovirus. Liquid amplification was performed until a high titer stock was used for protein production. Pellets of SF9 cells infected by the baculovirus were lysed in lysis buffer [25 mM Tris (pH 8), 1 mM EDTA (pH 8), 10% glycerol, 300 mM NaCl and half a tablet of Cp25] and sonicated for times for 10 s on and 10 s off. Supernatant was incubated on a HisTrap FF column regenerated with 100 mM NiSO₄. The column was washed with lysis buffer and Lgd-His protein recovered with elution buffer [25 mM Tris (pH 8), 10% glycerol, 300 mM NaCl, half a tablet of Cp25 and 300 mM imidazol].

Kinase assay on purified Lgd protein

We first exchanged the buffer of purified Lgd using illustra-NAP-10 column Sephadex G-25DNA grade (GE Healthcare) with solution Exchange [50 mM NaCl, 5 mM EDTA, 50 mM Tris-HCl (pH 7.4) and 0.1% NP40] in order to dilute purified Lgd in PK buffer (NEB, pH 7.5) at 25°C [50 mM Tris-HCl (pH 7.4), 10 mM MgCl₂, 0.1 EDTA, 2 mM DTT and 0.01% Brij35].

Then, a Cdk1 kinase assay was performed as follows: 10 µg purified Lgd was incubated for 45 min at 30°C in the presence of 0.2 µg active CycB/Cdk1 (Merck) and a gradient of 0, 50, 100, 200 µM of ATP (Sigma Aldrich) in PK buffer, to a final volume of 50 µl. Reactions were analyzed by western blotting and mass spectrometry (Institut Jacques Monod-Université Diderot). For the western blot, 45 µl of kinase assay reaction was added to 15 µl of Laemmli (4×) and denatured at 95°C for 10 min, and 20 µl of the sample were separated on 4-15% gradient mini-protean TGX precast gels (Bio-Rad) at 200 V and transferred using Tans-Blot Turbo mini nitrocellulose transfer packs (Bio-Rad). The membranes were blocked for 2 h at room temperature in blocking buffer (TBS, 0.1% Tween 20 and 5% BSA) and incubated overnight at 4°C in blocking buffer containing primary antibodies at the following dilution: mouse anti-MPM2 (05-368, Merck, 1:1000) and mouse anti-histidine (6605-1-Ig, Proteintech, 1:3000). After washes in TBS-T (TBS, 0.1% Tween20), membranes were incubated for 1 h in blocking buffer containing a peroxidase-conjugated anti-rabbit or anti-mouse IgG (Jackson ImmunoResearch) diluted at 1:10,000. After washes in TBS-T, bands were detected with the ECL Prime Western Blotting Detection Reagents (GE

Healthcare) and visualized using a mini-LAS-4000 Imaging System (Fujifilm). One gel was colored with Coomassie Blue for 2 h to detected all proteins.

Western blots on embryos extracts (Fig. S2A)

0 h to 12 h-old embryos were bleach-dechorionated and lysed in lysis buffer [50 mM Tris (pH 7.4), 150 mM NaCl, 0.1% NP40, 1 mM EDTA (pH 8), 1 mM DTT, 1×Complete EDTA-free Protease inhibitor cocktail (Roche) and 2×PhosSTOP Phosphatase inhibitor cocktail (Roche)] for 30 min at 4°C under rotation at 30 rpm. After 20 min of centrifugation at 16,000 *g* at 4°C, 300 µl of lysate was added to 100 µl of Laemmli (4×) and denatured at 95°C for 10 min. Samples were separated on 4-15% gradient mini-protean TGX precast gels (Bio-Rad) at 200 V and transferred using Tans-Blot Turbo mini nitrocellulose transfer packs (Bio-Rad). Membranes were blocked for 2 h at room temperature in blocking buffer (TBS, 0.1% Tween 20 and 5% BSA) and incubated overnight at 4°C in blocking buffer containing the primary antibodies at the following dilutions: rabbit anti-Lgd (a kind gift from Juergen Knoblich, IMBA, Vienna; 1:1000) or anti-peanut (4C9H4 anti-peanut, DSHB, 1:200). After washes in TBS-T (TBS, 0.1% Tween20), membranes were incubated for 1 h in blocking buffer containing peroxidase-conjugated anti-rabbit secondary antibody (111-035-003, Jackson ImmunoResearch; 1:10,000). After washes in TBS-T, bands were detected with the ECL Prime Western Blotting Detection Reagents (GE Healthcare) and visualized using a fusion FX to detect weak signal.

Quantification and statistics

Stem-cysts quantification was carried out on germaria immunostained using anti- α -spectrin antibody; stem-cysts were identified as a group of three cells minimum, linked by a fusome, with its most anterior cell being attached to the niche. Three experiments were quantified, and their mean and s.e.m. are represented. Unpaired *t*-tests were used.

Fluorescence intensity of GFP-Lgd at the midbody was calculated from the mean intensity measured in Fiji in a region of interest (ROI) at the midbody zone minus a ROI of the same size (15 pixels×15 pixels) in the cytoplasmic zone of the same cell. Unpaired *t*-tests were used to compare the fluorescence intensity measured in the different genotypes.

Quantification of Shrub-HA at the ring canal was carried out on germaria immunostained with anti- α -spectrin and anti-HA antibodies. The percentage of germline stem cells (GSCs) with localization of Shrub-HA at the ring canal was calculated. Three experiments were quantified, and their mean and s.e.m. are represented. Unpaired *t*-tests were used for comparisons.

Fluorescence intensity measurements of CHMP2B-GFP were carried out on *z*-stack images acquired with identical settings. A ROI, smaller than a ring canal (RC) width was chosen. For each RC, the mean intensity of three distinct ROIs was quantified using Fiji software. Row datasets were transformed into graphics with prism8 software. Wilcoxon-Mann-Whitney tests were used to compare fluorescence intensity.

Microscopy

Acquisitions of *z*-stacks on fixed samples were carried out using a Zeiss LSM780 or LSM980 confocal microscope.

Acknowledgements

We thank J. Knoblich, K. Haglund, the Bloomington Stock center and the DSHB for reagents used in this study. We thank R. Margueron for advice on protein expression and purification. We thank A. Echard for discussions and suggestions, and the Huynh lab for helpful comments on the manuscript. We are grateful to the Orion Imaging Facility (Collège de France) and BDD Curie Imaging facility. We thank the Institut Jacques Monod proteomic facility for the mass-spectrometry analyses. We also thank the imaging facility of Institut Curie PICT-IBISA Imaging platform, the imaging Facility ORION Technological core of CIRB and the proteomic platform ProteoSeine Core Facility of Institut Jacques Monod.

Competing interests

The authors declare no competing or financial interests.

Author contributions

Conceptualization: C.H., N.R.M., J.-R.H., J.M.; Methodology: N.R.M., P.M.-H., J.-R.H., J.M.; Validation: P.M.-H., J.-R.H., J.M.; Formal analysis: C.H., N.R.M., P.M.-H., J.M.; Investigation: C.H., N.R.M., P.M.-H., J.M.; Resources: J.-R.H., J.M.;

Data curation: C.H., N.R.M., J.-R.H., J.M.; Writing - original draft: C.H., J.M.; Writing - review & editing: J.-R.H., J.M.; Visualization: C.H., N.R.M., J.-R.H., J.M.; Supervision: J.-R.H., J.M.; Project administration: J.-R.H.; Funding acquisition: J.-R.H.

Funding

The J.-R.H. lab is supported by the Centre national de la recherche scientifique (CNRS), the Institut national de la santé et de la recherche médicale (INSERM), the Collège de France, La Fondation pour la Recherche Médicale (FRM) (Equipes FRM DEQ20160334884), the Agence Nationale de la Recherche (ANR) (ANR-15-CE13-0001-01, AbsCyStem) and the Fondation Bettencourt Schueller. C.H. was supported by an Agence Nationale de la Recherche post-doctoral fellowship (PDF20151203612).

Data availability

All relevant data can be found within the article and its [supplementary information](#).

Peer review history

The peer review history is available online at <https://journals.biologists.com/dev/lookup/doi/10.1242/dev.202306.reviewer-comments.pdf>

References

- Ables, E. T. and Drummond-Barbosa, D.** (2013). Cyclin E controls Drosophila female germline stem cell maintenance independently of its role in proliferation by modulating responsiveness to niche signals. *Development* **140**, 530-540. doi:10.1242/dev.088583
- Addi, C., Presle, A., Frémont, S., Cuvelier, F., Rocancourt, M., Milin, F., Schmutz, S., Chamot-Rooke, J., Douché, T., Duchateau, M. et al.** (2020). The Flemmingsome reveals an ESCRT-to-membrane coupling via ALIX/syntenin/syndecan-4 required for completion of cytokinesis. *Nat. Commun.* **11**, 1941. doi:10.1038/s41467-020-15205-z
- Andrade, V. and Ecard, A.** (2022). Mechanics and regulation of cytokinetic abscission. *Front. Cell Dev. Biol.* **10**, 1046617. doi:10.3389/fcell.2022.1046617
- Baeumers, M., Schulz, K. and Klein, T.** (2022). Using Drosophila melanogaster to analyse the human paralogs of the ESCRT-III core component Shrub/CHMP4/Snf7 and its interactions with members of the LGD/CC2D1 family. *Int. J. Mol. Sci.* **23**, 7507. doi:10.3390/ijms23147507
- Brand, A. H. and Perrimon, N.** (1993). Targeted gene expression as a means of altering cell fates and generating dominant phenotypes. *Development* **118**, 401-415. doi:10.1242/dev.118.2.401
- Buratovich, M. A. and Bryant, P. J.** (1997). Enhancement of overgrowth by gene interactions in lethal(2)giant discs imaginal discs from Drosophila melanogaster. *Genetics* **147**, 657-670. doi:10.1093/genetics/147.2.657
- Byers, T. J., Dubreuil, R., Branton, D., Kiehart, D. P. and Goldstein, L. S.** (1987). Drosophila spectrin. II. Conserved features of the alpha-subunit are revealed by analysis of cDNA clones and fusion proteins. *J. Cell Biol.* **105**, 2103-2110. doi:10.1083/jcb.105.5.2103
- Carlton, J. G. and Martin-Serrano, J.** (2007). Parallels between cytokinesis and retroviral budding: a role for the ESCRT machinery. *Science* **316**, 1908-1912. doi:10.1126/science.1143422
- Chou, T. B. and Perrimon, N.** (1992). Use of a yeast site-specific recombinase to produce female germline chimeras in Drosophila. *Genetics* **131**, 643-653. doi:10.1093/genetics/131.3.643
- Christ, L., Wenzel, E. M., Liestøl, K., Raiborg, C., Campsteijn, C. and Stenmark, H.** (2016). ALIX and ESCRT-III function as parallel ESCRT-III recruiters in cytokinetic abscission. *J. Cell Biol.* **212**, 499-513. doi:10.1083/jcb.201507009
- Clarke, A. L., Lettman, M. M. and Audhya, A.** (2022). Lgd regulates ESCRT-III complex accumulation at multivesicular endosomes to control intraluminal vesicle formation. *Mol. Biol. Cell* **33**, ar144. doi:10.1091/mbc.E22-08-0342
- de Cuevas, M. and Spradling, A. C.** (1998). Morphogenesis of the Drosophila fusome and its implications for oocyte specification. *Development* **125**, 2781-2789. doi:10.1242/dev.125.15.2781
- Eikenes, Å. H., Malerød, L., Christensen, A. L., Steen, C. B., Mathieu, J., Nezis, I. P., Liestøl, K., Huynh, J.-R., Stenmark, H. and Haglund, K.** (2015). ALIX and ESCRT-III coordinately control cytokinetic abscission during germline stem cell division in vivo. *PLoS Genet.* **11**, e1004904. doi:10.1371/journal.pgen.1004904
- Elia, N., Sougrat, R., Spurlin, T. A., Hurley, J. H. and Lippincott-Schwartz, J.** (2011). Dynamics of endosomal sorting complex required for transport (ESCRT) machinery during cytokinesis and its role in abscission. *Proc. Natl Acad. Sci. USA* **108**, 4846-4851. doi:10.1073/pnas.1102714108
- Goliand, I., Nachmias, D., Gershony, O. and Elia, N.** (2014). Inhibition of ESCRT-II-CHMP6 interactions impedes cytokinetic abscission and leads to cell death. *Mol. Biol. Cell* **25**, 3740-3748. doi:10.1091/mbc.e14-08-1317
- Guizetti, J., Schermelleh, L., Mäntler, J., Maar, S., Poser, I., Leonhardt, H., Müller-Reichert, T. and Gerlich, D. W.** (2011). Cortical constriction during abscission involves helices of ESCRT-III-dependent filaments. *Science* **331**, 1616-1620. doi:10.1126/science.1201847
- Gulluni, F., Prever, L., Li, H., Krafčikova, P., Corrado, I., Lo, W.-T., Margaria, J. P., Chen, A., De Santis, M. C., Cnudde, S. J. et al.** (2021). PI(3,4)P2-mediated cytokinetic abscission prevents early senescence and cataract formation. *Science* **374**, eabk0410. doi:10.1126/science.abk0410
- Laporte, M. H., Chatellard, C., Vauchez, V., Hemming, F. J., Deloulme, J.-C., Vossier, F., Blot, B., Fraboulet, S. and Sadoul, R.** (2017). Alix is required during development for normal growth of the mouse brain. *Sci. Rep.* **7**, 44767. doi:10.1038/srep44767
- Mathieu, J. and Huynh, J. R.** (2017). Monitoring complete and incomplete abscission in the germ line stem cell lineage of Drosophila ovaries. *Methods Cell Biol.* **137**, 105-118. doi:10.1016/bs.mcb.2016.03.033
- Mathieu, J., Cauvin, C., Moch, C., Radford, S. J., Sampaio, P., Perdigoto, C. N., Schweisguth, F., Bardin, A. J., Sunkel, C. E., McKim, K. et al.** (2013). Aurora B and cyclin B have opposite effects on the timing of cytokinesis abscission in Drosophila germ cells and in vertebrate somatic cells. *Dev. Cell* **26**, 250-265. doi:10.1016/j.devcel.2013.07.005
- Mathieu, J., Michel-Hissier, P., Boucherit, V. and Huynh, J.-R.** (2022). The deubiquitinase USP8 targets ESCRT-III to promote incomplete cell division. *Science* **376**, 818-823. doi:10.1126/science.abg2653
- Matias, N. R., Mathieu, J. and Huynh, J.-R.** (2015). Abscission is regulated by the ESCRT-III protein shrub in Drosophila germline stem cells. *PLoS Genet.* **11**, e1004653. doi:10.1371/journal.pgen.1004653
- McMillan, B. J., Tibbe, C., Drabek, A. A., Seegar, T. C. M., Blacklow, S. C. and Klein, T.** (2017). Structural basis for regulation of ESCRT-III complexes by Lgd. *Cell reports* **19**, 1750-1757. doi:10.1016/j.celrep.2017.05.026
- Morawa, K. S., Schneider, M. and Klein, T.** (2015). Lgd regulates the activity of the BMP/Dpp signalling pathway during Drosophila oogenesis. *Development* **142**, 1325-1335. doi:10.1242/dev.112961
- Morita, E., Sandrin, V., Chung, H.-Y., Morham, S. G., Gygi, S. P., Rodesch, C. K. and Sundquist, W. I.** (2007). Human ESCRT and ALIX proteins interact with proteins of the midbody and function in cytokinesis. *EMBO J.* **26**, 4215-4227. doi:10.1038/sj.emboj.7601850
- Nakamura, A., Naito, M., Arai, H. and Fujita, N.** (2010). Mitotic phosphorylation of Aki1 at Ser208 by cyclin B1-Cdk1 complex. *Biochem. Biophys. Res. Commun.* **19**, 872-876. doi:10.1016/j.bbrc.2010.02.103
- Ni, J.-Q., Zhou, R., Czech, B., Liu, L.-P., Holderbaum, L., Yang-Zhou, D., Shim, H.-S., Tao, R., Handler, D., Karpowicz, P. et al.** (2011). A genome-scale shRNA resource for transgenic RNAi in Drosophila. *Nat. Methods* **8**, 405-407. doi:10.1038/nmeth.1592
- Pfützner, A.-K., Mercier, V., Jiang, X., Moser von Filseck, J., Baum, B., Šarić, A. and Roux, A.** (2020). An ESCRT-III polymerization sequence drives membrane deformation and fission. *Cell* **182**, 1140-1155.e1118. doi:10.1016/j.cell.2020.07.021
- Pfützner, A.-K., Moser von Filseck, J. and Roux, A.** (2021). Principles of membrane remodeling by dynamic ESCRT-III polymers. *Trends Cell Biol.* **31**, 856-868. doi:10.1016/j.tcb.2021.04.005
- Sarov, M., Barz, C., Jambor, H., Hein, M. Y., Schmied, C., Suchold, D., Stender, B., Janosch, S., KJ, V. V., Krishnan, R. T. et al.** (2016). A genome-wide resource for the analysis of protein localisation in Drosophila. *eLife* **5**, e12068. doi:10.7554/eLife.12068
- Stoten, C. L. and Carlton, J. G.** (2018). ESCRT-dependent control of membrane remodelling during cell division. *Semin. Cell Dev. Biol.* **74**, 50-65. doi:10.1016/j.semcdb.2017.08.035
- Troost, T., Jaeckel, S., Ohlenhard, N. and Klein, T.** (2012). The tumour suppressor Lethal (2) giant discs is required for the function of the ESCRT-III component Shrub/CHMP4. *J. Cell Sci.* **125**, 763-776. doi:10.1242/jcs.097261
- Vaccari, T., Rusten, T. E., Menut, L., Nezis, I. P., Brech, A., Stenmark, H. and Bilder, D.** (2009). Comparative analysis of ESCRT-I, ESCRT-II and ESCRT-III function in Drosophila by efficient isolation of ESCRT mutants. *J. Cell Sci.* **122**, 2413-2423. doi:10.1242/jcs.046391
- Van Doren, M., Williamson, A. L. and Lehmann, R.** (1998). Regulation of zygotic gene expression in Drosophila primordial germ cells. *Curr. Biol.* **8**, 243-246. doi:10.1016/S0960-9822(98)70091-0
- Ventimiglia, L. N., Cuesta-Geijo, M. A., Martinelli, N., Caballe, A., Macheboeuf, P., Miguet, N., Parnham, I. M., Olmos, Y., Carlton, J. G., Weissenhorn, W. et al.** (2018). CC2D1B coordinates ESCRT-III Activity during the mitotic reformation of the nuclear envelope. *Dev. Cell* **47**, 547-563.e546. doi:10.1016/j.devcel.2018.11.012
- Vietri, M., Radulovic, M. and Stenmark, H.** (2019). The many functions of ESCRTs. *Nat. Rev. Mol. Cell Biol.* **21**, 25-42. doi:10.1038/s41580-019-0177-4
- Villa-Fombuena, G., Lobo-Pecellin, M., Marin-Menguiano, M., Rojas-Ríos, P. and González-Reyes, A.** (2021). Live imaging of the Drosophila ovarian niche shows spectroscopy and centrosome dynamics during asymmetric germline stem cell division. *Development* **148**, dev199716. doi:10.1242/dev.199716